AGU PUBLICATIONS

Earth and Space Science

RESEARCH ARTICLE
10.1002/2016EA000248

Key Points:
- The NASA CERES surface and atmospheric radiative flux estimates are subject to the quality of NASA GMAO reanalysis used
- The assimilation of DYNAMO observations improves vertical profiles of local atmospheric humidity and temperature in the GMAO reanalysis
- The improved atmospheric humidity and temperature in the GMAO reanalysis improve CERES-like daily longwave estimates

Correspondence to:
H. Wang,
hailanw@gmail.com

Citation:
Wang, H., W. Su, N. G. Loeb, D. Achuthavarier, and S. D. Schubert (2017), The role of DYNAMO in situ observations in improving NASA CERES-like daily surface and atmospheric radiative flux estimates, *Earth and Space Science*, *4*, 164–183, doi:10.1002/2016EA000248.

Received 30 DEC 2016
Accepted 10 MAR 2017
Accepted article online 20 MAR 2017
Published online 3 APR 2017

The role of DYNAMO in situ observations in improving NASA CERES-like daily surface and atmospheric radiative flux estimates

Hailan Wang[1,2,3], Wenying Su[2], Norman G. Loeb[2], Deepthi Achuthavarier[3,4], and Siegfried D. Schubert[3]

[1]Science Systems and Applications, Inc, Hampton, Virginia, USA, [2]Climate Science Branch, NASA Langley Research Center, Hampton, Virginia, USA, [3]Global Modeling and Assimilation Office, NASA GSFC, Greenbelt, Maryland, USA, [4]Universities Space Research Association, Columbia, Maryland, USA

Abstract The daily surface and atmospheric radiative fluxes from NASA Clouds and the Earth's Radiant Energy System (CERES) Synoptic 1 degree (SYN1deg) Ed3A are among the most widely used data to study cloud-radiative feedback. The CERES SYN1deg data are based on Fu-Liou radiative transfer computations that use specific humidity (*Q*) and air temperature (*T*) from NASA Global Modeling and Assimilation Office (GMAO) reanalyses as inputs and are therefore subject to the quality of those fields. This study uses in situ *Q* and *T* observations collected during the Dynamics of the Madden-Julian Oscillation (DYNAMO) field campaign to augment the input stream used in the NASA GMAO reanalysis and assess the impact on the CERES daily surface and atmospheric longwave estimates. The results show that the assimilation of DYNAMO observations considerably improves the vertical profiles of analyzed *Q* and *T* over and near DYNAMO stations by moistening and warming the lower troposphere and upper troposphere and drying and cooling the mid-upper troposphere. As a result of these changes in *Q* and *T*, the computed CERES daily surface downward longwave flux increases by about 5 W m^{-2}, due mainly to the warming and moistening in the lower troposphere; the computed daily top-of-atmosphere (TOA) outgoing longwave radiation increases by 2–3 W m^{-2} during dry periods only. Correspondingly, the estimated local atmospheric longwave radiative cooling enhances by about 5 W m^{-2} (7–8 W m^{-2}) during wet (dry) periods. These changes reduce the bias in the CERES SYN1deg-like daily longwave estimates at both the TOA and surface and represent an improvement over the DYNAMO region.

1. Introduction

Cloud-radiative feedback is an important process involved in a number of weather and climate phenomena in the tropics. One such phenomenon is the Madden-Julian Oscillation (MJO), a leading mode of tropical intraseasonal variability that interacts with and influences a wide range of weather and climate extremes and represents a key source of subseasonal predictability [*Zhang*, 2005; *Waliser*, 2011]; past observational and modeling studies [e.g., *Sobel and Maloney*, 2012, 2013; *Wang et al.*, 2013, 2016] have demonstrated cloud-radiative feedback associated with moist convection as a key process for the existence of the MJO. Observational studies addressing relatively short time scale phenomena such as the MJO often require *daily* radiative flux observations at the top of the atmosphere (TOA), within the atmosphere and at the surface. While global daily TOA fluxes can be made available from satellite measurements [e.g., *Doelling et al.*, 2013], direct measurements of global daily surface and atmospheric radiative fluxes are lacking, particularly over the oceans. Satellite-based estimates of surface and atmospheric radiative fluxes rely on radiative transfer calculations, with cloud and aerosol input taken from imager retrievals and atmospheric state input obtained from reanalyses. The quality of such estimates thus depends upon the quality of the input cloud and atmospheric data, which may subsequently affect observational studies that use these data. The NASA Clouds and the Earth's Radiant Energy System (CERES) provides daily TOA and surface radiative fluxes in the Synoptic 1 degree (SYN1deg) Ed3A data product [*Doelling et al.*, 2013], which is widely used to study observed radiative processes and to calculate surface and atmospheric energy budgets [e.g., *Sobel et al.*, 2014]. The daily surface and atmospheric radiative fluxes in the SYN1deg Ed3A are produced by using the NASA Langley Fu-Liou radiative transfer model [*Fu and Liou*, 1992; *Rose et al.*, 2013], which uses Moderate Resolution Imaging Spectroradiometer (MODIS) and geostationary satellite cloud properties, and atmospheric profiles of specific humidity (*Q*) and air temperature (*T*) from NASA Global Modeling and

Assimilation Office (GMAO) reanalysis as inputs. The uncertainties in the SYN1deg fluxes computed with satellite-derived cloud and aerosol properties have been assessed by using MODIS-, Cloud-Aerosol Lidar and Infrared Pathfinder Satellite Observation-, and CloudSat-based cloud and aerosol products [*Kato et al.*, 2012], while the dependence of the SYN1deg computed fluxes on the quality of the GMAO reanalysis has not been well addressed.

Like all other reanalyses, the GMAO reanalysis is subject to the quality and quantity of the observations that are assimilated and any biases in the assimilating model. While global satellite observations are undoubtedly important in the reanalysis system, in situ conventional observations are essential, especially over regions where the assimilating model is deficient in simulating local physical processes (e.g., over the tropical oceans). In the absence of in situ observations, the reanalysis basic state variables are mostly constrained by satellite observations, which often have insufficient vertical resolution to correct biases in the vertical profiles of the model-generated first-guess fields. The assimilation of high-quality in situ observations can improve the reanalysis by drawing it closer to the observations. These in situ measurements can also be used to evaluate a reanalysis, as well as to help better identify and understand physical deficiencies in the assimilating model [e.g., *Mapes and Bacmeister*, 2012].

During the 2011–2012 winter (1 October 2011 to March 2012), Dynamics of the MJO (DYNAMO), the U.S. component of the Cooperative Indian Ocean experiment on intraseasonal variability in the Year 2011, collected in situ observations over the tropical Indian Ocean in order to focus on the convective initiation processes of the MJO. The unprecedented DYNAMO field campaign was motivated by the poor understanding of physical processes of MJO initiation over tropical Indian Ocean and the poor representation of the MJO in current atmospheric general circulation models (AGCMs). The DYNAMO campaign collected a number of key variables including specific humidity (Q) and air temperature (T), so as to promote an improved understanding of the MJO initiation processes. The in situ observations from the DYNAMO field campaign also provide an excellent opportunity to evaluate and improve current reanalyses over the tropical Indian Ocean.

Recently, we have produced two GMAO reanalyses that assimilate global observations with and without DYNAMO observations, referred to as the DYNAMO reanalysis and the control reanalysis, respectively [*Achuthavarier et al.*, 2017]. The goal of that work was to assess the impact of the DYNAMO observations on the GMAO reanalysis as well as to better identify and understand the physical bias in the assimilation model—the Goddard Earth Observing System Model, version 5 (GEOS 5) AGCM. By comparing these two reanalyses, *Achuthavarier et al.* [2017] performed a comprehensive assessment of the impact of the DYNAMO observations on the GMAO reanalysis. The results showed that the assimilation of DYNAMO observations brings the reanalysis basic state variables closer to the observed and considerably improves the GMAO reanalysis representation of the observed MJO initiation processes over the tropical Indian Ocean. Motivated by those results, the present study examines in more detail the impact of DYNAMO observations on the assimilated Q and T profiles and assesses the subsequent effect on CERES SYN1deg-like daily radiative flux estimates.

This paper is organized as follows. Section 2 describes the NASA CERES data, consisting of Energy Balanced and Filled (EBAF)-TOA Ed2.8, SYN1deg Ed3A and EBAF-Surface Ed2.8. It also describes the control and DYNAMO reanalyses, the DYNAMO gridded in situ observations, the Atmospheric Infrared Sounder (AIRS) data, and a series of Fu-Liou radiative transfer calculations designed to assess the effect of improvements in GMAO reanalysis Q and T on CERES SYN1deg daily longwave estimates. Section 3 presents our results on the improvement of T and Q in GMAO reanalysis from assimilating the DYNAMO observations and the subsequent effect on CERES SYN1deg-like longwave estimates. The summary and conclusions are provided in section 4.

2. Data and Methods

2.1. NASA EBAF-TOA Ed2.8, CERES SYN1deg Ed3A, and EBAF-Surface Ed2.8 Data

The NASA CERES data used in this study include EBAF-TOA Ed2.8 [*Loeb et al.*, 2009, 2012], SYN1deg Ed3A [*Doelling et al.*, 2013], and EBAF-Surface Ed2.8 [*Kato et al.*, 2013]. The EBAF-TOA Ed2.8 and EBAF-Surface Ed2.8 are available monthly only, whereas the SYN1deg Ed3A includes 3-hourly, daily, and monthly data. All these data are at a resolution of 1° latitude/longitude and are available from March 2000 onwards.

The CERES EBAF-TOA Ed2.8 [*Loeb et al.*, 2009, 2012] radiative fluxes are among the most widely used satellite-based observations of TOA fluxes; they consist of TOA incident solar flux and TOA upward shortwave and longwave radiative fluxes under clear-sky and all-sky conditions. The grid box mean of EBAF-TOA clear-sky fluxes are determined by using an area-weighted average of CERES/Terra broadband fluxes from completely cloud-free CERES footprints (20 km equivalent diameter at nadir), and the Moderate Resolution Imaging Spectroradiometer (MODIS)/Terra-derived "broadband" clear-sky fluxes (1 km) estimated from the cloud-free portions of partly and mostly cloudy CERES footprints. The use of high-resolution (1 km) MODIS data in producing the CERES EBAF-TOA clear-sky fluxes increases the sampling of clear-sky scenes over regions that are frequently cloudy and thereby lowers the sampling uncertainty. With an objective constrainment algorithm, the EBAF-TOA all-sky shortwave and longwave fluxes are adjusted within their range of uncertainty to remove the inconsistency between global net TOA flux and heat storage in the Earth-atmosphere system.

The CERES SYN1deg Ed3A [*Doelling et al.*, 2013] products include CERES-observed temporally interpolated TOA radiative fluxes and coincident MODIS-derived cloud and aerosol properties, along with geostationary-derived cloud properties and broadband fluxes that have been carefully normalized with CERES TOA fluxes for consistency with CERES. They also contain computed untuned daily TOA, in-atmosphere, and surface fluxes, produced by using the Langley Fu-Liou radiative transfer model [*Rose et al.*, 2013]. The Fu-Liou computations use MODIS and geostationary satellite cloud properties along with atmospheric profiles provided by an older version of the GMAO reanalysis (tag: GEOSadas-4_1 for data processing of months prior to January 2008 and GEOSadas-5_2_0 for January 2008 and months after that) and are subject to errors in the input data. During the DYNAMO period (1 October 2011 to 31 March 2012), the GMAO reanalysis used in the SYN1deg Ed3A assimilates some of the DYNAMO observations. The DYNAMO observations assimilated are real-time Global Telecommunication System (GTS) submissions and thus lack postfield quality checks and a variety of corrections that address a number of data quality issues discussed in *Ciesielski et al.* [2014a]; these data are also of relatively low vertical resolution (15–25 hPa). An evaluation of the SYN1deg Ed3A [*Rutan et al.*, 2015] using surface observations at 85 globally distributed land (37) and ocean buoy (48) sites along with several other global surface observations across 8 years (2000–2007) shows a bias of 3.0 W m^{-2} for computed surface downward shortwave flux and a bias of -4.0 W m^{-2} for computed surface downward longwave flux. The evaluation over the ocean (land) sites shows a bias of 4.9 W m^{-2} (1.8 W m^{-2}) for computed surface downward shortwave flux and a bias of -3.6 W m^{-2} (-4.2 W m^{-2}) for computed surface downward longwave flux.

The CERES EBAF-Surface Ed2.8 [*Kato et al.*, 2013] consists of surface upward and downward shortwave and longwave radiative fluxes under all-sky and clear-sky conditions. They are produced based on the computed untuned monthly TOA fluxes from the SYN1deg Ed3A. The SYN1deg Ed3A computed untuned TOA fluxes do not necessarily agree with those from the EBAF-TOA Ed2.8 observations, in part because of the errors in the inputs used in the Fu-Liou computations. The SYN1deg Ed3A computed untuned surface fluxes are also affected by the input data errors. To produce EBAF-Surface fluxes with minimal errors, an objective constrainment algorithm is used to adjust surface, atmospheric, and cloud properties within their uncertainties in order to ensure that the computed TOA fluxes are consistent with the EBAF-TOA fluxes within their observational error. Such adjustment considerably reduces the bias and root-mean-square error for surface downward longwave flux over both ocean and land, and surface downward shortwave flux over ocean [*Kato et al.*, 2013].

2.2. NASA GEOS 5 Data Assimilation System

Both the control and DYNAMO reanalyses (see also section 2.3) used in this study are produced by using the NASA GEOS 5 data assimilation system (DAS) for the Modern-Era Retrospective analysis for Research and Applications, version 2 (MERRA-2) (DAS tag: GEOSadas-5_12_4) [*Bosilovich et al.*, 2015], though at a coarser 1° resolution. The GEOS 5 DAS integrates the GEOS 5 AGCM with the Gridpoint Statistical Interpolation analysis, jointly developed by the NOAA/National Centers for Environmental Prediction (NCEP) and NASA/GMAO. The satellite radiance data are directly assimilated by using the Joint Center for Satellite Data Assimilation Community Radiative Transfer Model, and variational bias correction is used for radiances. The primary performance drivers for the GEOS 5 DAS are temperature and moisture fields suitable for the Earth Observing System instrument teams, wind fields for transport studies of the stratospheric and tropospheric

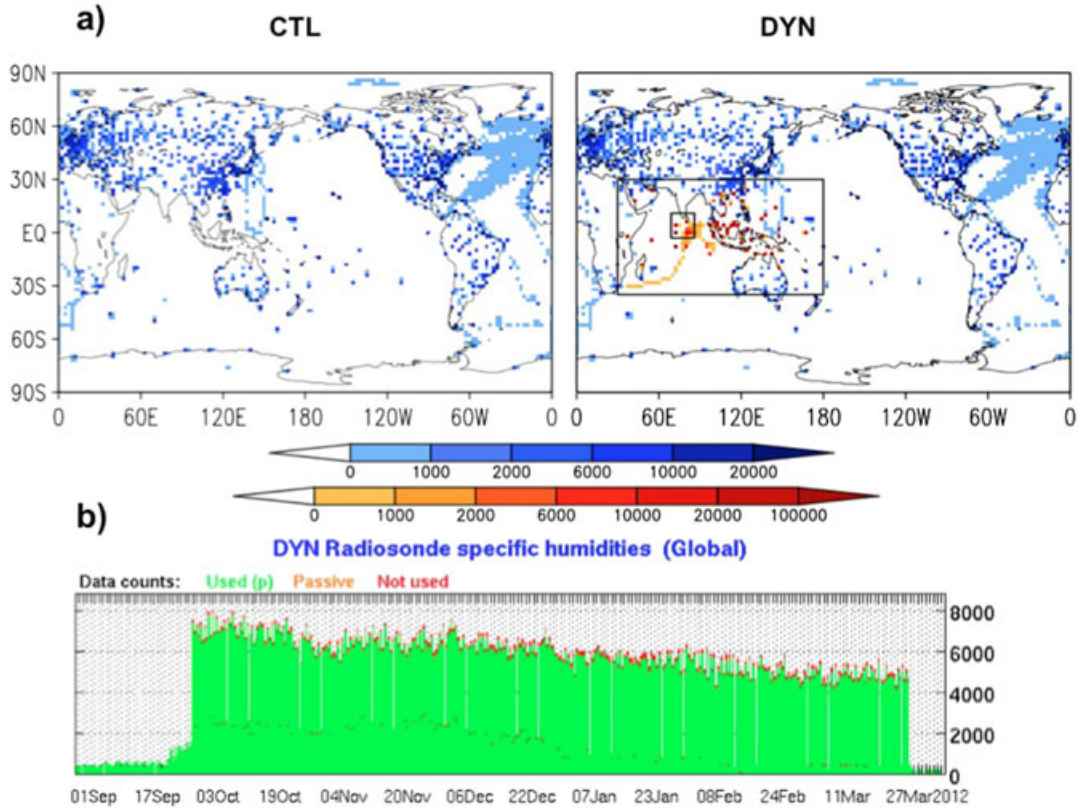

Figure 1. (a) Mean radiosonde specific humidity data counts for 1 October 2011 to 31 March 2012 and all vertical pressure levels combined, for the control reanalysis (top left) and the DYNAMO reanalysis (top right). The red shading indicates DYNAMO stations, and the blue the regular. On the top right plot, the DYNAMO domain is indicated by a large rectangle and the small rectangle covers the Northern Sounding Array region. (b) The DYNAMO radiosonde specific humidity observation data count for all vertical levels combined as a function of time, where the green section shows used data and the yellow and red sections represent passive and rejected data. From *Achuthavarier et al.* [2017].

chemistry communities, and climate-quality analyses to support studies of the hydrological cycle (e.g., MERRA-2). Incremental Analysis Updates [*Bloom et al.*, 1996] is used to constrain the assimilating model with observations by slowly adjusting the model states toward the observed states throughout the 6 h analysis period [*Rienecker et al.*, 2008]. The GEOS 5 AGCM [*Rienecker et al.*, 2008; *Molod et al.*, 2012] employs the finite-volume dynamics of *Lin* [2004], integrated with various moist physics packages [*Bacmeister et al.*, 2006] that include a modified form of the Relaxed Arakawa-Schubert convection scheme [*Moorthi and Suarez*, 1992] with stochastic Tokioka limits on plume entrainment [*Tokioka et al.*, 1988], prognostic cloud microphysics [*Bacmeister et al.*, 2006], and the Catchment Land Surface Model [*Koster et al.*, 2000].

2.3. The Control and DYNAMO Reanalyses

In order to assess the impact of DYNAMO observations on the GMAO reanalysis, we have produced both a 1° DYNAMO reanalysis and a 1° control reanalysis, which assimilate global observations with and without the DYNAMO observations, respectively [*Achuthavarier et al.*, 2017]. The DYNAMO observations used in the DYNAMO reanalysis consist of level 4 radiosonde, pibal GTS resolution wind data, and Priority Sounding Site (PSS) and Non-Priority Sounding Site (NPSS) GTS resolution data, all downloaded from the DYNAMO data website (http://data.eol.ucar.edu/master_list/?project=DYNAMO). These DYNAMO observations have undergone rigorous quality checks to remove a variety of data issues [*Ciesielski et al.*, 2014b]. The temporal coverage of the assimilated DYNAMO observations reflects the changes in DYNAMO data collection frequency (Figure 1c): it shows considerably larger data counts during October 2011 to November 2011, a gradual reduction during December 2011, and further decreased data counts afterward. In the control reanalysis, all the DYNAMO observations, including those at the DYNAMO enhanced stations and the PSS and the NPSS stations, have been removed (Figure 1b). This is to make the contrast between the control reanalysis

and the DYNAMO reanalysis as distinct as possible. Both reanalyses were produced over the DYNAMO period (1 October 2011 to 31 March 2012). *Achuthavarier et al.* [2017] provides more information on how these reanalyses were produced.

It is worth noting here that the 1° DYNAMO reanalysis uses the observational error table for MERRA instead of that for MERRA-2. The MERRA error table specifies smaller observational error for radiosonde than the MERRA-2 error table. This places an overall stronger constraint to radiosonde observations and thus draws the DYNAMO reanalysis closer to the quality-controlled DYNAMO observations, allowing us to better assess the subsequent effect on the CERES SYN1deg-like surface and atmospheric radiative flux estimates.

In this study, we focus on the first half of the DYNAMO period (1 October to 31 December 2011), during which there are abundant DYNAMO observations. This period also had three convective events occurring during October, November, and December 2011, respectively [*Yoneyama et al.*, 2013; *Johnson and Ciesielski*, 2013], allowing us to investigate the dependence of our results on dry and wet periods.

2.4. The DYNAMO Gridded Observations and NASA AIRS Data

The fidelity of the control and DYNAMO reanalyses is investigated by comparing their specific humidity and air temperature profiles against those in the DYNAMO gridded in situ observations version 3a [*Johnson and Ciesielski*, 2013; *Ciesielski et al.*, 2014a, 2014b] and the NASA Atmospheric Infrared Sounder (AIRS)/Advanced Microwave Sounding Unit (AMSU-A), version 6 (V6) Level 3 (L3) data (AIRX3STM.006) [*Aumann et al.*, 2003; *Chahine et al.*, 2006; *Tian et al.*, 2013b] over DYNAMO stations.

The DYNAMO gridded observations are available 3-hourly from 1 October to 31 December 2011. Using the multiquadric interpolation scheme from *Nuss and Titley* [1994], the data are made available at 1° latitude/longitude with a vertical resolution of 25 hPa from 1000 hPa up to 50 hPa. Extensive postfield phase processing of the radiosonde data have been performed to correct a variety of data issues (e.g., daytime dry bias, errors in baseline surface data, and ship deck heating effects), with considerable efforts targeted improving the quality of humidity observations [*Ciesielski et al.*, 2014b]. The DYNAMO gridded observations are constructed without using any model analyses and as such are devoid of any model issues (e.g., model parameterizations). They are used as an independent data to evaluate reanalyses and satellite-based observations.

The AIRS/AMSU V6 L3 gridded specific humidity and air temperature [*Tian et al.*, 2013a] are based on the combined retrievals from AIRS and AMSU. The AIRS data have global coverage with humidity and temperature measurements co-located with each other. Due to the limitations of the AIRS (infrared) and AMSU (microwave) instruments, however, there are no retrievals for regions with cloud fraction above 70%, resulting in low sampling in cloudy regions; the AIRS sampling also varies with latitude, and the diurnal cycle coverage is incomplete [*Tian et al.*, 2013b]. The sampling differences between the AIRS and reanalyses could explain a considerable portion of their regional differences, particularly those over tropical deep convective regions [e.g., *Tian et al.*, 2013a]. Despite these limitations, the AIRS specific humidity and air temperature have been widely used for various observational studies. In CERES EBAF-Surface Ed2.8 data production, the AIRS data (AIRX3STM.006) is used for an initial correction of upper tropospheric relative humidity; it is also used to determine the uncertainty of GMAO reanalysis temperature and humidity, which is subsequently used for a Lagrange multiplier process to match computed TOA irradiances with CERES-derived TOA irradiances [*Kato et al.*, 2013]. The AIRS V6 L3 data are available monthly, at a resolution of 1° latitude/longitude, with 12 standard layers from 1000 hPa to 100 hPa for specific humidity, and 24 standard pressure levels from 1000 hPa to 1 hPa for air temperature.

2.5. Fu-Liou Radiative Transfer Calculations

The Fu-Liou radiative transfer model used in this study is based on the original Fu-Liou model [*Fu and Liou*, 1992] and was further developed at the NASA Langley Research Center [*Rose et al.*, 2013]. For the SYN1deg Ed3A daily data production, the input for the Fu-Liou radiative transfer calculations includes 3-hourly satellite-based cloud and aerosol properties, surface albedo, and Q and T from GMAO reanalyses produced by using older versions of the GMAO DAS (tag: GEOSadas-4_1 prior to January 2008 and GEOSadas-5_2_0 on and after January 2008).

Table 1. The List of Fu-Liou Radiative Transfer Experiments Performed[a]

Experiment	Specific Humidity (*Q*)	Air Temperature (*T*)	Rest Daily Inputs
Control	Control	Control	From SYN1deg Ed3A
DYNAMO	DYNAMO	DYNAMO	
Q	DYNAMO	Control	
Qlo	Use DYNAMO if DYNAMO is wetter than Control below 600 hPa	Control	
Qmi	Use DYNAMO if DYNAMO is drier than Control between 200 hPa and 800 hPa	Control	
Qhi	Use DYNAMO if DYNAMO is wetter than Control above 400 hPa	Control	
T	Control	DYNAMO	
Tlo	Control	Use DYNAMO if DYNAMO is warmer than Control below 600 hPa	
Tmi	Control	Use DYNAMO if DYNAMO is cooler than Control between 200 hPa and 800 hPa	
Thi	Control	Use DYNAMO if DYNAMO is warmer than Control above 400 hPa	

[a]These experiments differ from each other only in the daily specific humidity (*Q*) and air temperature (*T*) used, with the rest daily inputs all taken from CERES SYN1deg Ed3A. For brevity, in the columns for "specific humidity (*Q*)" and "air temperature (*T*)," the control and DYNAMO reanalyses are referred to as "Control" and "DYNAMO," respectively.

In order to assess the effect of changes in reanalysis *T* and *Q* on SYN1deg-like daily radiative flux estimates, we performed a series of Fu-Liou radiative transfer experiments for the first half of the DYNAMO period (1 October to 31 December 2011) (Table 1). The control and DYNAMO Fu-Liou experiments use daily *T* and *Q* from the control reanalysis and the DYNAMO reanalysis, respectively, with the rest of daily input (e.g., cloud properties) identical to each other, all taken from the SYN1deg Ed3A. The comparison of the control and DYNAMO Fu-Liou experiments thus quantifies the impact of reanalysis *T* and *Q* changes (from the DYNAMO data assimilation) on the SYN1deg-like radiative flux estimates. As will be shown in section 3.1, the assimilation of the DYNAMO observations mainly improves the vertical profiles of reanalysis *Q* and *T*. Since these *T* and *Q* changes in different vertical pressure ranges often reflect reanalysis improvement in representing discrete physical processes (e.g., shallow convection in the lower troposphere), we further performed a series of Fu-Liou experiments (Q, Qhi, Qmi, Qlo, T, Thi, Tmi, and Tlo) in order to determine the separate contributions of *T* and *Q* improvements in the upper troposphere, middle troposphere, and lower troposphere to the overall improvement in the SYN1deg-like daily radiative flux estimates. These Fu-Liou experiments are identical to the control Fu-Liou experiment except that we use *T* or *Q* from the DYNAMO reanalysis for selected vertical pressure ranges (e.g., surface–600 hPa, 600 hPa–300 hPa, and 250 hPa–TOA) (Table 1). Further, we performed two additional Fu-Liou experiments, which use monthly mean *T* and *Q* from the DYNAMO gridded observations and the AIRS, respectively, over the DYNAMO stations in the central tropical Indian Ocean. These experiments are used to assess whether the longwave estimate differences between the DYNAMO and control Fu-Liou experiments represent an improvement. In all the Fu-Liou experiments performed, the aerosol type is set as sea salt and the aerosol optical thickness is prescribed as 0.12, following MODIS-based observations over the tropical Indian Ocean during cold seasons. We note that for the control and DYNAMO Fu-Liou experiments, we have also performed a set of parallel Fu-Liou runs, using 3-hourly atmosphere and four-layer cloud input from the SYN1deg Ed3A. The results (not shown) are quite similar to those using the daily mean input in Table 1, suggesting that the effect of the diurnal cycle of the input fields on the daily mean radiative flux estimates is small overall.

Because of the various differences between our Fu-Liou computations and those in the standard SYN1deg Ed3A data production, particularly the use of different GMAO reanalyses and aerosol settings, we do not compare the absolute values of computed radiative fluxes. We instead mainly focus on the differences of the computed radiative fluxes between our Fu-Liou experiments in Table 1.

3. Results

3.1. Impact of DYNAMO Observations on *Q* and *T* in the GMAO Reanalysis

The assimilation of 5 hPa vertical resolution DYNAMO in situ observations in the GMAO DAS presumably improves the GMAO reanalysis by constraining the basic state variables to the DYNAMO observations,

particularly the vertical profiles of *Q* and *T*. This section examines the impact of DYNAMO observations by comparing *Q* and *T* from the control reanalysis with those from the DYNAMO reanalysis.

Figures 2 and 3 illustrate the horizontal and vertical distribution of changes in October–December mean *Q* and *T* due to the assimilation of the DYNAMO observations, obtained by subtracting the control reanalysis from the DYNAMO reanalysis. The impact of the DYNAMO observations on *Q* and *T* is primarily local, located over and nearby the DYNAMO stations (Figure 2). The most obvious impact is on the vertical profile of *Q* and *T* in the tropical Indian Ocean (Figure 3). Relative to the control reanalysis, the assimilation of the DYNAMO observations in the DYNAMO reanalysis moistens the lower troposphere (near surface and about 800 hPa) by up to 4% and dries the middle troposphere (peak between 500 hPa and 600 hPa) by about 8%. While the moistening in the upper troposphere is not as noticeable because atmospheric water vapor decreases rapidly with height, the DYNAMO reanalysis shows an increase of about 6% relative to the control reanalysis (Figure 3b). To investigate whether the above changes in *Q* represent an improvement, we examine in Figure 3c the analysis tendency for specific humidity from the DYNAMO reanalysis. Here the analysis tendency is a term used in the GEOS 5 data assimilation system to nudge model forecast in the direction of the observations and thus reflects the influence of the assimilated observations; since the GEOS 5 AGCM computes the tendency due to dynamics relatively accurately, the analysis tendency term largely reflects errors in model physics but with an opposite sign [*Mapes and Bacmeister*, 2012]. The vertical distribution of the analysis tendency for specific humidity in Figure 3c indicates that relative to all the observations assimilated, the GEOS 5 AGCM has a dry (wet) bias in the lower (middle) troposphere, so that atmospheric moisture needs to be added (removed) in order to bring the reanalysis closer to the observations assimilated. The comparison between Figures 3b and 3c suggests that the assimilation of the DYNAMO observations improves the vertical profile of reanalysis *Q* by moistening (drying) the lower (middle) troposphere, partially overcoming the dry (wet) bias there in the GEOS 5 AGCM, thereby bringing the reanalysis closer to the DYNAMO observations.

The impact of the DYNAMO observations on the vertical profile of T (Figures 3d–3f) is considerable. The assimilation of DYNAMO observations (Figure 3e) warms the lower troposphere (surface and near 700 hPa) and upper troposphere (around 200 hPa) and cools the mid-upper troposphere (around 350 hPa) and lower stratosphere (around 100 hPa), by up to 0.5 K. These effects of the DYNAMO observations contribute significantly to overcoming the GEOS 5 AGCM biases. Figure 3f shows that the model biases consist of cold biases in the lower troposphere (near surface and around 700 hPa) and upper troposphere (100–150 hPa) as well as a warm bias in the mid-upper troposphere (between 200–500 hPa). The DYNAMO observations help correct the model bias by about 25% in the middle and upper troposphere and account for ~80% of the model *T* correction in the lower troposphere.

To further investigate whether the impact of the DYNAMO observations on reanalysis *Q* and *T* has any dependence on MJO phase (i.e., dry, transitional, and wet periods), we first examine in Figure 4 the temporal distribution of *Q* and *T* differences between the control and DYNAMO reanalyses averaged over the central tropical Indian Ocean during 1 October to 31 December 2011. Despite weather noise and the development of three convective events, the general features of monthly *Q* and *T* differences in Figure 3 are present throughout much of the period and do not appear to show strong dependence on MJO phase. To better quantify the extent to which the impact of DYNAMO observations on reanalysis *T* and *Q* depends on MJO phase, we followed *Kim et al*. [2014] and computed composites of specific humidity profile binned by precipitation percentiles for both the control and DYNAMO reanalyses, using their respective gridded daily specific humidity and precipitation data over the central tropical Indian Ocean during 1 October to 31 December 2011. Here the precipitation percentile provides a measure of MJO phase, among which the dry suppressed, transitional, and deep convective phases correspond to $<$50%, 50–85%, and $>$85% of precipitation percentiles, respectively. The probability distribution function of precipitation is overall similar between the control and the DYNAMO reanalyses [*Achuthavarier et al*., 2017]. Figure 5 shows that the MJO phase dependence of the *Q* and *T* changes due to the assimilation of the DYNAMO observations is weak overall. The assimilation of DYNAMO observations moistens the lower troposphere (near surface, around 800 hPa) and upper troposphere by up to 4% and 6%, respectively, and dries the middle troposphere (around 500 hPa) by ~2%. The lower tropospheric moistening and midtropospheric drying are more prominent during the deep convective phase. The results for the analysis tendency for *Q* in Figure 5c show that the GEOS 5 AGCM has a dry bias in

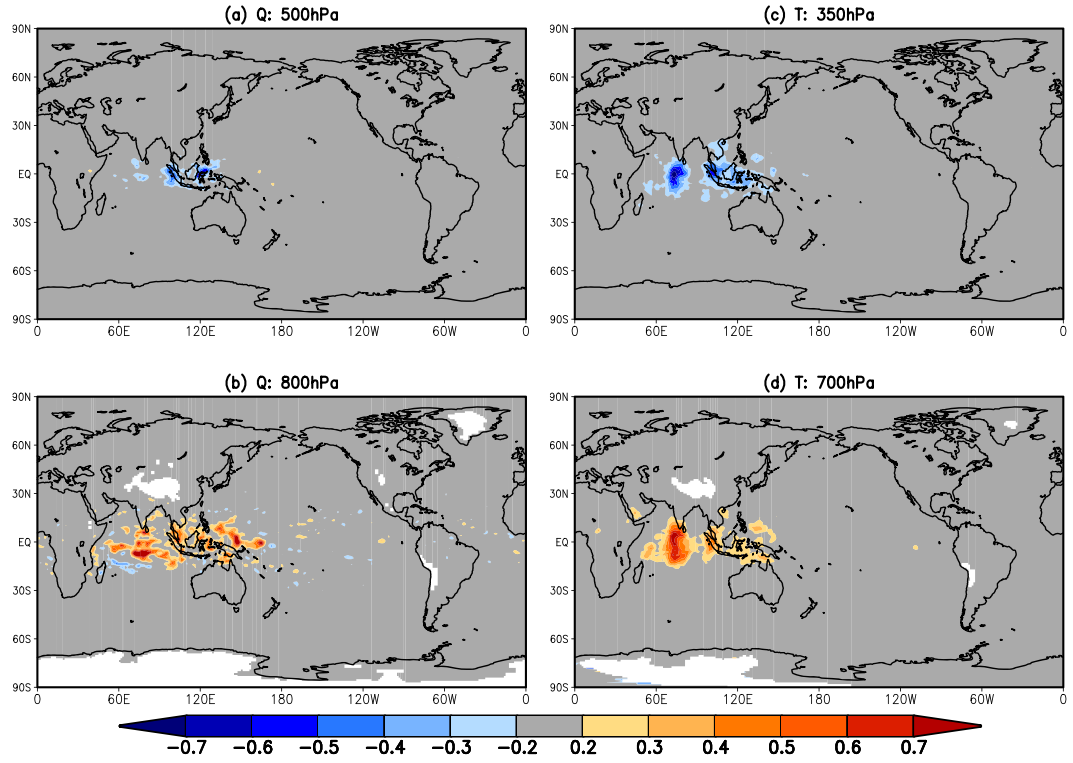

Figure 2. The 1 October to 31 December 2011 mean differences between the DYNAMO reanalysis and the control reanalysis (DYNAMO minus control) for specific humidity (g kg^{-1}) at (a) 500 hPa and (b) 800 hPa, and air temperature (K) at (c) 350 hPa and (d) 700 hPa.

the lower troposphere (peak at 850 hPa) and a wet bias in the middle troposphere (peak at 450 hPa). These biases are present for most precipitation percentiles, with the magnitude peaking during the transitional zones between dry and wet regimes, while they are reduced for very dry and deep convective regimes. We note that the composite results for the transitional regimes in Figure 5 do not differentiate between dry-to-wet transition and wet-to-dry transition. A composite relative to the MJO phase such as rainfall peak [e.g., *Del Genio and Chen*, 2015] would be more informative, as the physical processes during the dry-to-wet transition (MJO active phase) differ from those during the wet-to-dry-transition (MJO decay phase). The rather limited MJO sample size during the period of 1 October to 31 December 2011, however, makes such composite analysis less reliable.

The effect of the DYNAMO observations on *T* is much more distinct than on *Q* (Figures 5e and 5f). The assimilation of DYNAMO observations warms the lower troposphere (below 650 hPa, 0.4 K) and upper troposphere near 200 hPa (0.2 K), while cooling the mid-upper troposphere (300–500 hPa) and further above (100 hPa) by up to 0.4 K. The above changes in *T* show little dependence on MJO phases. These changes contribute to overcoming model warm bias in the mid-upper troposphere (around 300 hPa) and cold bias in the upper troposphere (around 150 hPa) by about 25% and are the primary contributor to correcting model cold bias in the lower troposphere (near surface, and 700 hPa). It is worth noting that the dry and cold GEOS 5 AGCM biases in the lower troposphere are a reflection of model deficiencies in the simulation of tropical shallow convection. The GEOS 5 AGCM uses the relaxed Arakawa-Schubert scheme to produce moist convection. While the scheme performs well in producing deep convection, it does less well for shallow convection (Andrea Molod 2016, personal communication). This makes it difficult for the model to simulate the observed MJO initiation processes, during which the transition from shallow convection to deep convection is critical [e.g., *Hagos et al.*, 2014]. The contribution of the DYNAMO observations in correcting the model cold and dry biases in the lower troposphere suggests the importance of assimilating DYNAMO-like in situ observations in a reanalysis, especially when the assimilating GCM is deficient in simulating the observed moist physical processes. Note that other reanalyses are also influenced by their assimilating models and display various vertical biases of *Q* and *T* over the tropical Indian Ocean. The European Centre for Medium-Range Weather

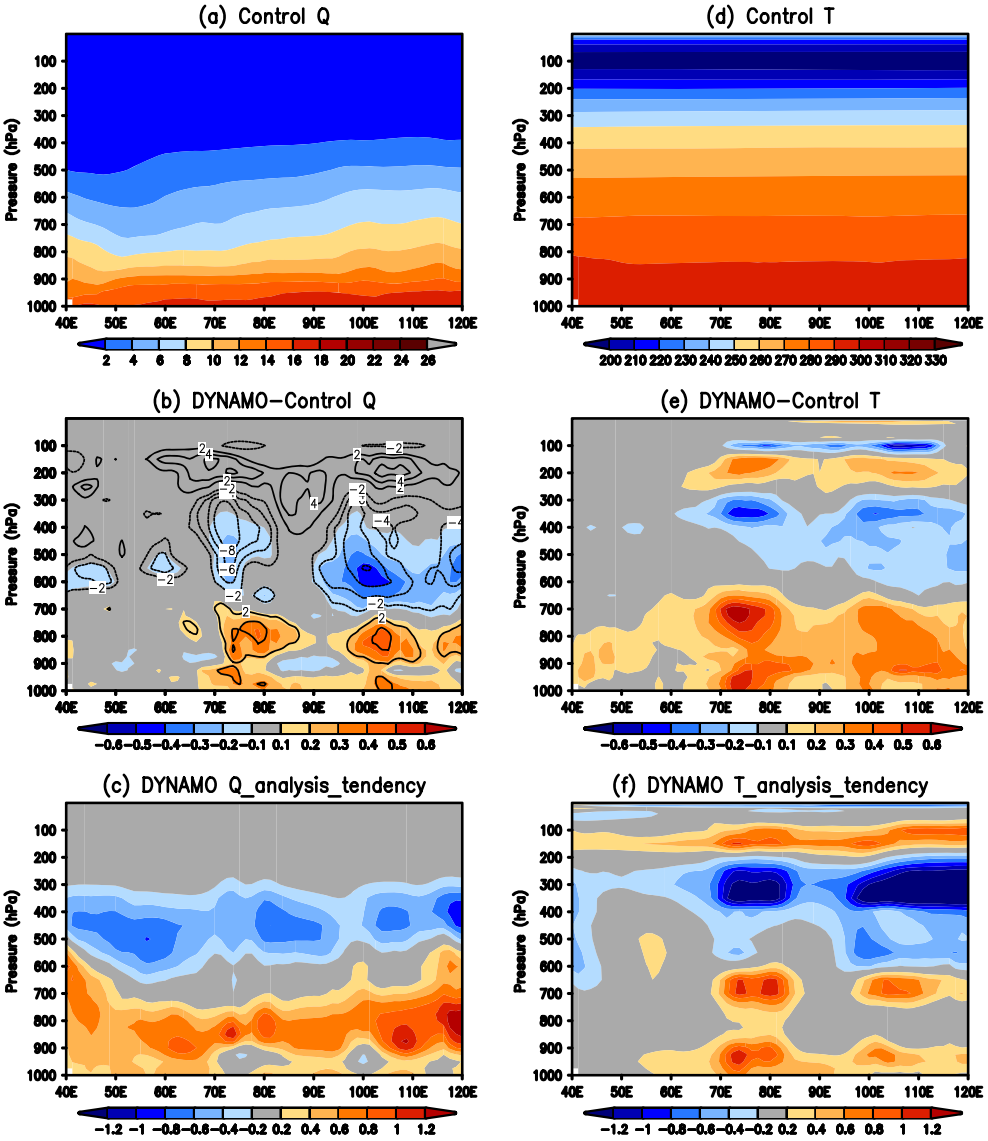

Figure 3. (a) The vertical profile of 1 October to 31 December 2011 mean of specific humidity (g kg^{-1}) averaged between 5°S and 10°N in the control reanalysis. (b) Same as Figure 3a but for specific humidity difference (g kg^{-1}) between the DYNAMO reanalysis and the control reanalysis (DYNAMO minus control), with black contours indicating the relative change (%) from the control reanalysis to the DYNAMO reanalysis. (c) Same as Figure 3a but for analysis tendency for specific humidity (g m^{-2} d^{-1}) in the DYNAMO reanalysis. (d–f) Same as Figures 3a–3c but for air temperature. Units are in K in Figures 3d and 3e and in K d^{-1} in Figure 3f.

Forecasts operational analyses show a low-level (1000–750 hPa) cold bias, a dry bias below 950 hPa, and a wet bias between 950 and 750 hPa [*Nagarajan and Aiyyer*, 2004]. The NCEP Global Forecast System (GFS) analysis has a notable dry bias in the boundary layer and a moist bias near 750 hPa at Gan Island, which may result from an overactive shallow cumulus parameterization scheme that removes too much boundary layer moisture and deposits it further above [*Ciesielski et al.*, 2014a]. The GFS analysis also displays cold biases near 100 hPa and warm biases near 250 hPa, which could result from radiative effects related to excessive reanalysis moisture and cloudiness between 100 and 200 hPa.

3.2. Effect on CERES SYN1deg-Like Daily Radiative Flux Estimates

Given the above improvement in reanalysis *Q* and *T* from the DYNAMO observation assimilation, particularly their vertical profiles, this section investigates the extent to which these changes in *Q* and *T* subsequently affect the CERES SYN1deg-like daily surface and atmospheric radiative flux estimates. Here the effects of *Q*

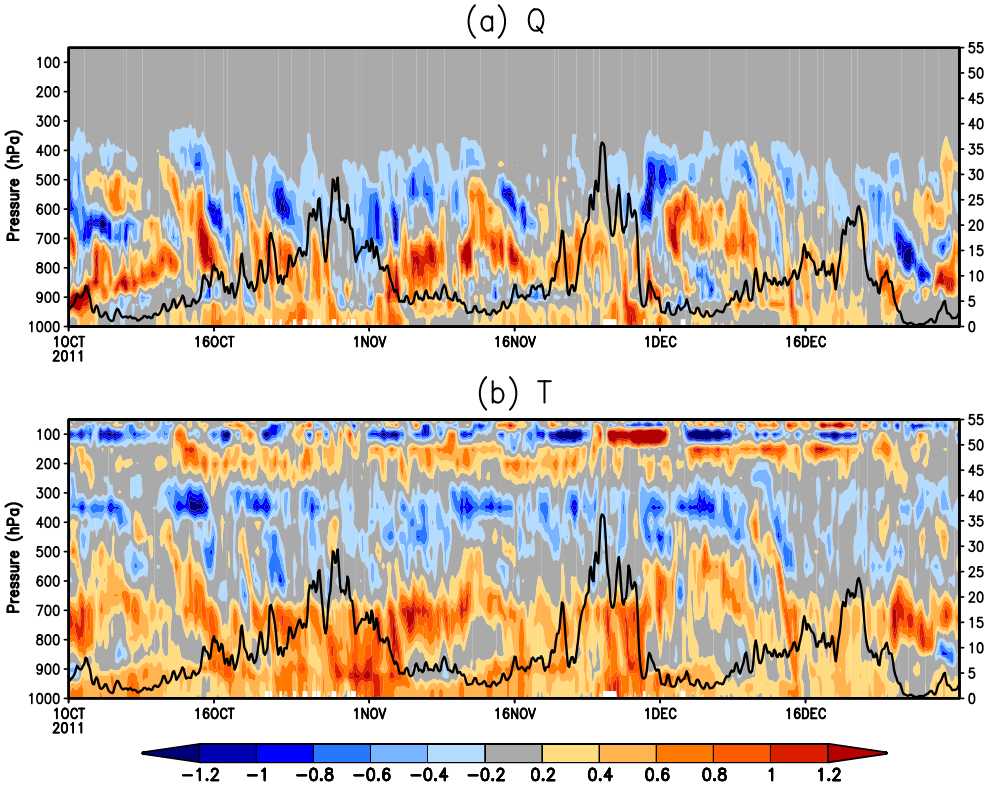

Figure 4. (a) The temporal evolution of specific humidity (shaded, g kg^{-1}) and precipitation (mm d^{-1}) (black line) differences between the DYNAMO reanalysis and the control reanalysis (DYNAMO minus control) averaged over the central tropical Indian Ocean (70°E–82°E, 5°S–10°N). The thin black contours indicate the relative change (%) from the control reanalysis to the DYNAMO reanalysis. (b) Same as Figure 4a but for air temperature (K).

and *T* changes are assessed by contrasting the results from the Fu-Liou radiative transfer experiments listed in Table 1. The changes in *Q* and *T* mainly affect surface downward longwave flux; their effects on shortwave and surface upward longwave fluxes are minimal. Thus, this section only presents the results for surface downward longwave.

We first examine in Figure 6 the regional distribution of October–December 2011 mean outgoing longwave radiation (OLR) and surface downward longwave flux in the control Fu-Liou experiment, for all-sky and clear-sky conditions, as well as the corresponding cloud-radiative effects (CRE). Here the TOA CRE is defined as clear-sky OLR minus all-sky OLR, whereas the surface downwelling CRE is obtained as all-sky surface downward longwave minus its clear-sky component. We focus on the Indian Ocean and western Pacific, as that is where the impact of the DYNAMO observations dominates (Figure 2). At the TOA, the all-sky OLR shows a minimum over the tropical Indo-Pacific warm pool region where the deep convective clouds absorb and reemit the infrared radiation emitted from the Earth's surface, with larger values outside that region where there are less clouds. The clear-sky OLR shows a minimum over the tropical Indo-Pacific as well, but its gradient between the warm pool region and the surrounding regions is much smaller than that of the all-sky OLR. The minimum clear-sky OLR over the warm pool region is largely associated with the warm and moist atmosphere there relative to other regions. The TOA longwave CRE in the control Fu-Liou calculation (42.7 W m^{-2}) is comparable to that in the EBAF TOA Ed2.8 (41.8 W m^{-2}) over the tropical Indo-Pacific warm pool region (60°E–160°E, 15°S–15°N). While not shown here, the TOA longwave CRE (Figure 6c) agrees with the CERES SYN1deg Ed3A high cloud amount (300 hPa–tropopause) in spatial pattern, which reflects the overall contribution of TOA radiative effects of high clouds during deep convective periods.

The impact of the tropical Indo-Pacific warm pool is clearly shown in the surface downward longwave as well. Relative to the other regions, the deep convective clouds and the warm and moist atmosphere over the warm pool emit more infrared radiation downward and lead to greater longwave radiation reaching the surface (Figure 6d). The clear-sky surface downward longwave (Figure 6e) is overall similar to its all-sky

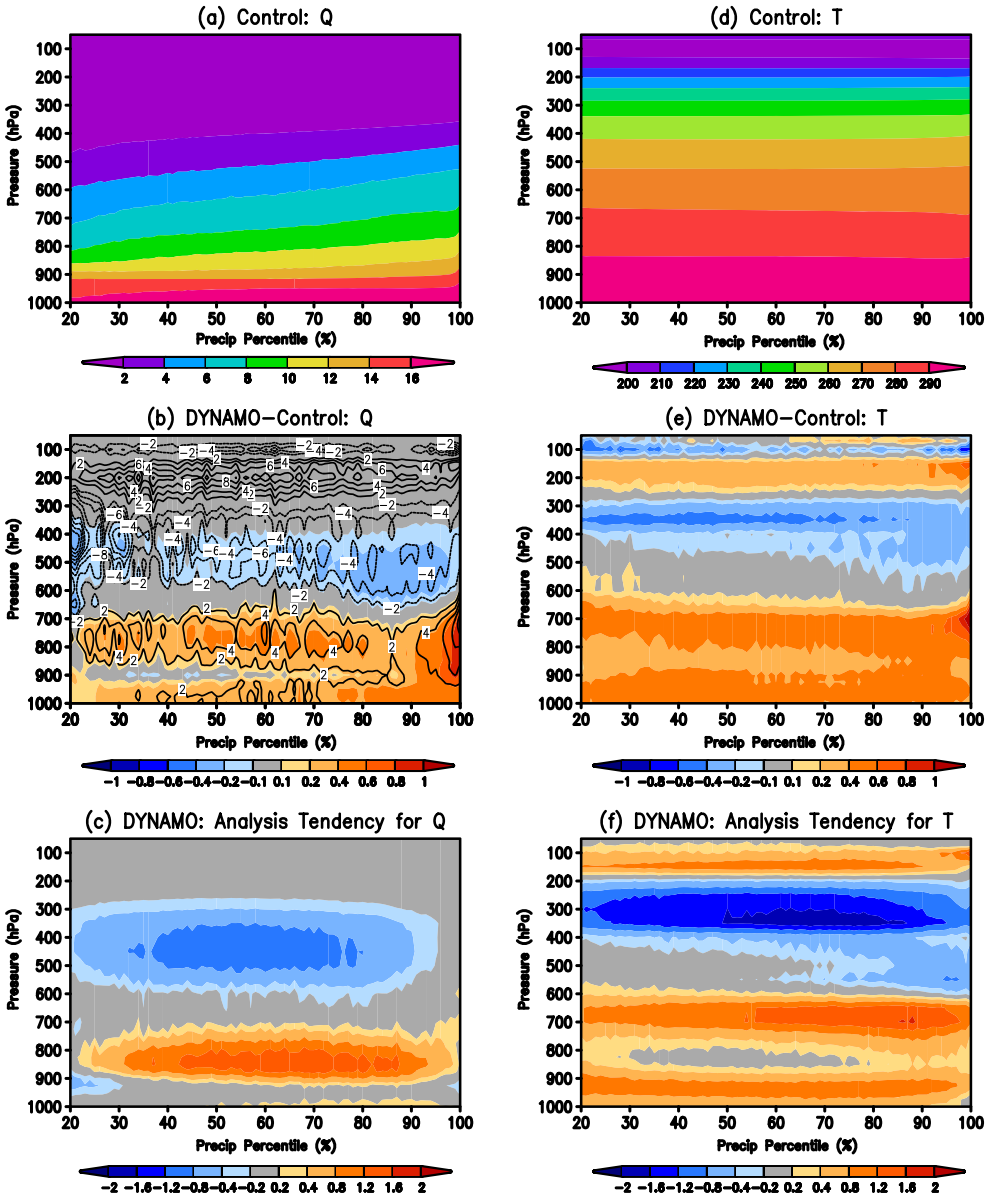

Figure 5. (a) The vertical profile of specific humidity (g kg^{-1}) composites as a function of precipitation percentile, computed by using gridded daily data over the central tropical Indian Ocean (70°E–82°E, 5°S–10°N) during 1 October to 31 December 2011. (b) Same as Figure 5a but for the specific humidity composite difference between the DYNAMO reanalysis and the control reanalysis (DYNAMO minus control); the black contours indicate the relative change (%) from the control reanalysis to the DYNAMO reanalysis. (c) Same as Figure 5a but for the analysis tendency for specific humidity (g m^{-2} s^{-1}). (d–f) Same as Figures 5a–5c but for air temperature. Units are in K in Figures 5d and 5e and in K d^{-1} in Figure 5f.

component in spatial pattern, except that it displays a more uniform distribution. The corresponding surface downward longwave CRE is weak overall, especially over the warm pool where the all-sky and clear-sky downward longwave are comparable to each other.

The effects of the improved *Q* and *T* in the GMAO reanalysis (Figures 2 and 3) on the SYN1deg-like computed daily longwave are investigated by comparing the control and DYNAMO Fu-Liou experiments. Figure 7 shows their differences averaged over the period of 1 October to 31 December 2011. At the TOA (Figures 7a–7c), the improved *T* and *Q* leads to an increase of 1 W m^{-2} (2 W m^{-2}) in computed all-sky (clear-sky) OLR over and near the DYNAMO stations, resulting in an increase of 1 W m^{-2} TOA longwave CRE locally. The effect of the *T* and *Q* changes on the computed surface downward all-sky longwave (Figure 7d) is much greater than at the TOA (Figure 7a). They lead to an increase of 5 W m^{-2} over the central tropical Indian Ocean and an

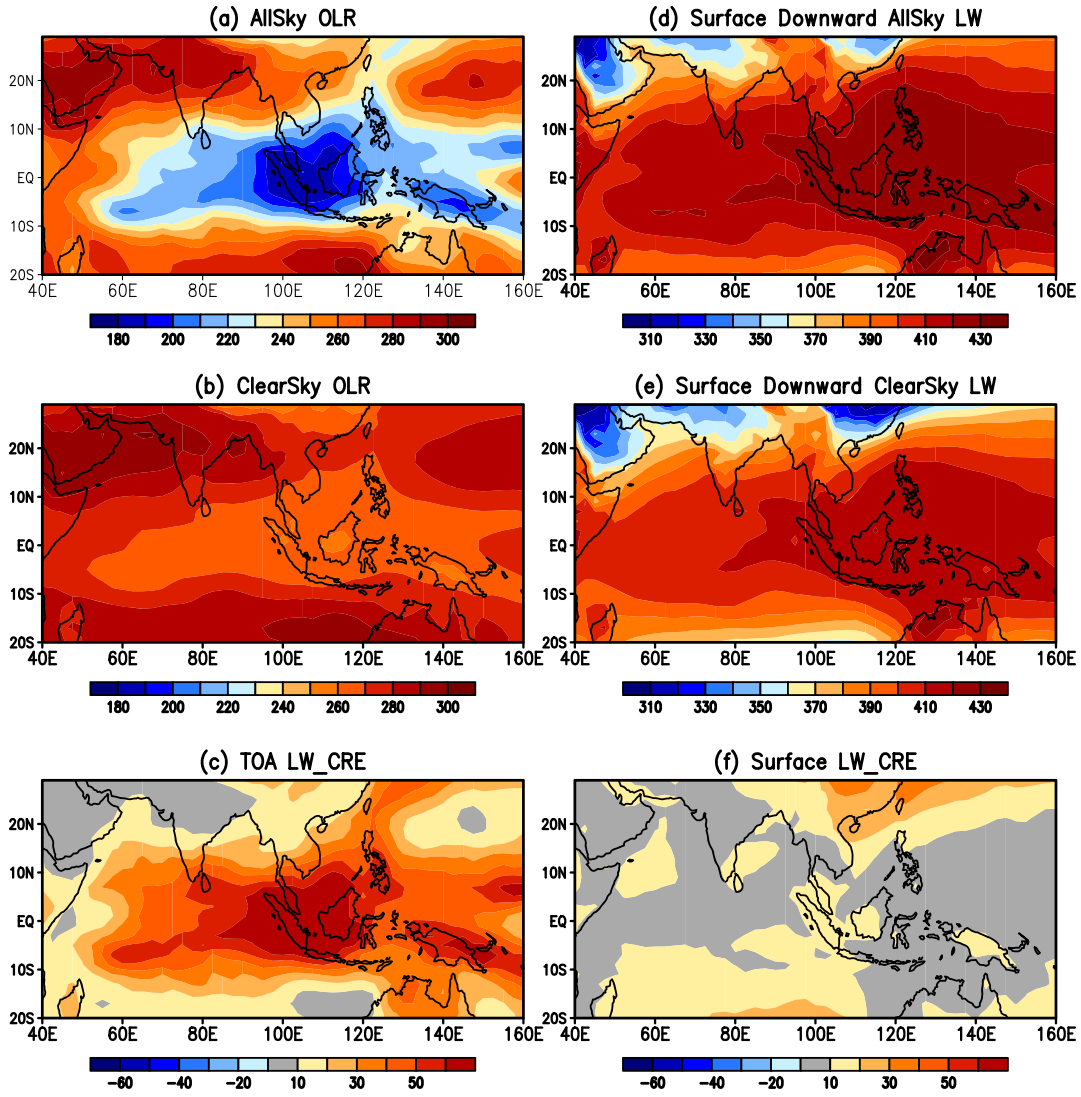

Figure 6. The 1 October to 31 December 2011 mean of (a) all-sky OLR, (b) clear-sky OLR, (c) TOA longwave CRE, (d) surface downward all-sky longwave, (e) surface downward clear-sky longwave, and (f) surface longwave CRE, from the control Fu-Liou experiment. Units are in W m^{-2}.

increase of 2 W m^{-2} over and near the Maritime continent (Figure 7d). The effect on the clear-sky surface downward longwave (Figure 7e) is similar overall to its all-sky component, resulting in little change in the surface downward longwave CRE (Figure 7f).

The 1 October to 31 December 2011 mean distribution in Figure 7 essentially combines dry and wet events altogether. It is of interest to further examine whether the changes in the computed daily longwave have any dependence on dry and wet phases. Figure 8 illustrates the temporal evolution of all-sky OLR, clear-sky OLR, and the corresponding TOA longwave CRE over the central tropical Indian Ocean (5°S–10°N). Here we focus on features over and north of the equator, as that is where MJO signals dominate [*Johnson and Ciesielski*, 2013]. Figure 8a clearly illustrates the three eastward propagating convective events during 1 October to 31 December 2011. The changes in *T* and *Q* only affect the computed all-sky OLR during dry and transitional periods, during which they lead to an increase of 3 W m^{-2}; their effects are small overall during the deep convective periods, as the all-sky OLR is largely controlled by deep convective clouds then. The effect on clear-sky OLR (Figure 8c) is persistent throughout much of the period, during which the computed daily clear-sky OLR increases by about 3 W m^{-2}. As a result, the estimate of TOA longwave CRE increases by up to 3 W m^{-2} during convective periods, while remaining unchanged during dry and transitional periods.

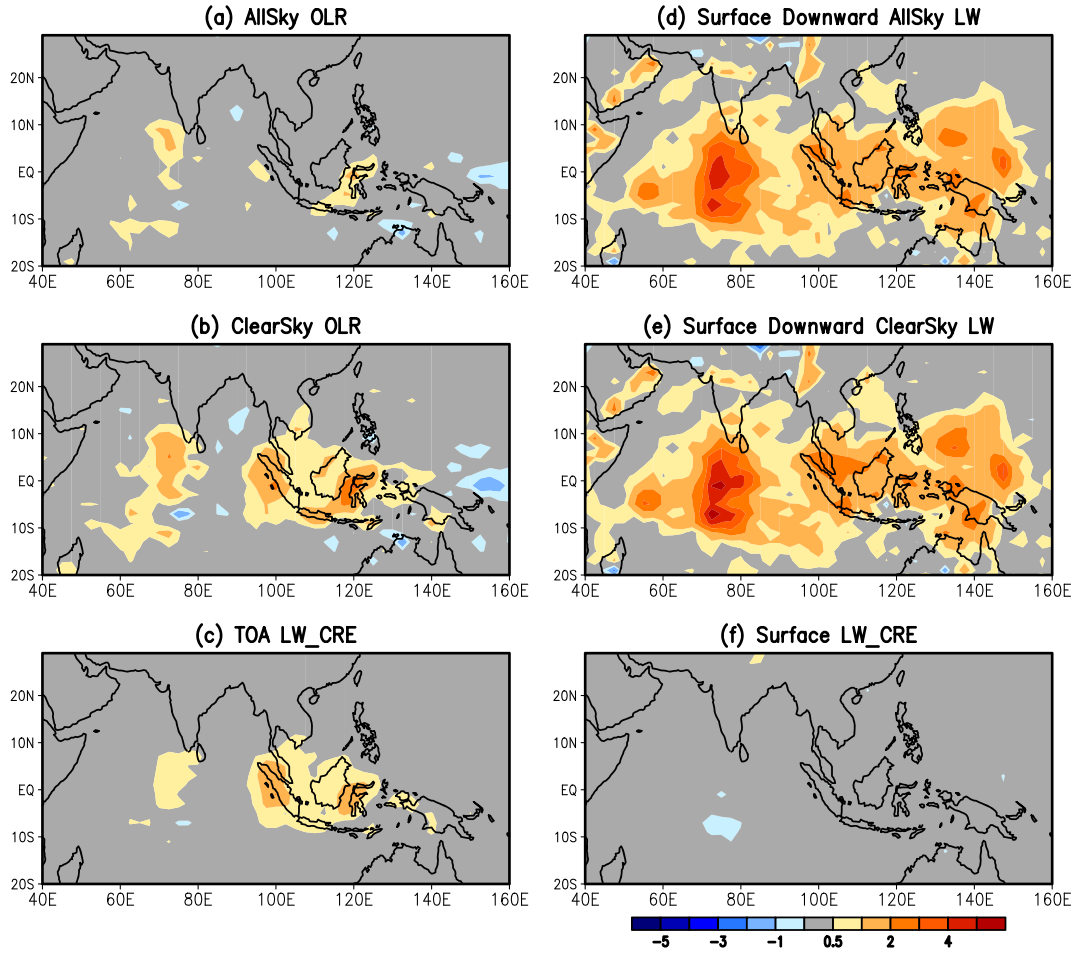

Figure 7. The 1 October to 31 December 2011 mean difference between the DYNAMO and control Fu-Liou experiments (DYNAMO minus control) (see Table 1) for (a) all-sky OLR, (b) clear-sky OLR, (c) TOA longwave CRE, (d) surface downward all-sky longwave, (e) surface downward clear-sky longwave, and (f) surface longwave CRE. Units are in W m^{-2}.

Figure 8 also suggests that the effect of *T* and *Q* changes on monthly mean TOA longwave depends on the relative length or duration of dry and wet periods: it tends to be greater for a month dominated by dry days than by wet days.

We next examine in Figure 9 the effect of *T* and *Q* changes on the computed daily surface downward longwave over the central tropical Indian Ocean (5°S–10°N). Figure 9a clearly shows the effect of deep convective clouds during the three convective events, during which the warm convective cloud base leads to more downward longwave radiation reaching the surface. The effect of *Q* and *T* changes on surface downward all-sky longwave flux (Figure 9b) is quite distinct, which shows an increase of up to 8 W m^{-2} over and near DYNAMO stations throughout much of the period. The results for clear-sky longwave (Figure 9c) strongly resemble those for all-sky longwave (Figure 9b), resulting in a rather small change in surface downward longwave CRE. The dependence on dry and wet phases is weak overall.

We note that these longwave flux estimate improvements are about 1 order smaller than individual terms in daily column-integrated Moist Static Energy (MSE) budget and thus may not impact discussions of daily MSE budget in past studies that use the CERES SYN1deg Ed3A [e.g., *Sobel et al.*, 2014]. The daily fluctuations of column net radiative heating used in the MSE budget analysis, defined as the differences between the net radiative fluxes at the TOA and surface, are dominated by those of TOA upward shortwave flux, TOA OLR, and surface downward shortwave flux, the magnitudes of which are often greater than 100 W m^{-2}. By comparison, the magnitude of daily fluctuations of surface downward longwave flux is about 10 W m^{-2}. At daily time scale, the impact of the longwave estimate improvement is significant for surface downward longwave flux, but considerably less so for atmospheric longwave flux and net atmospheric radiative fluxes.

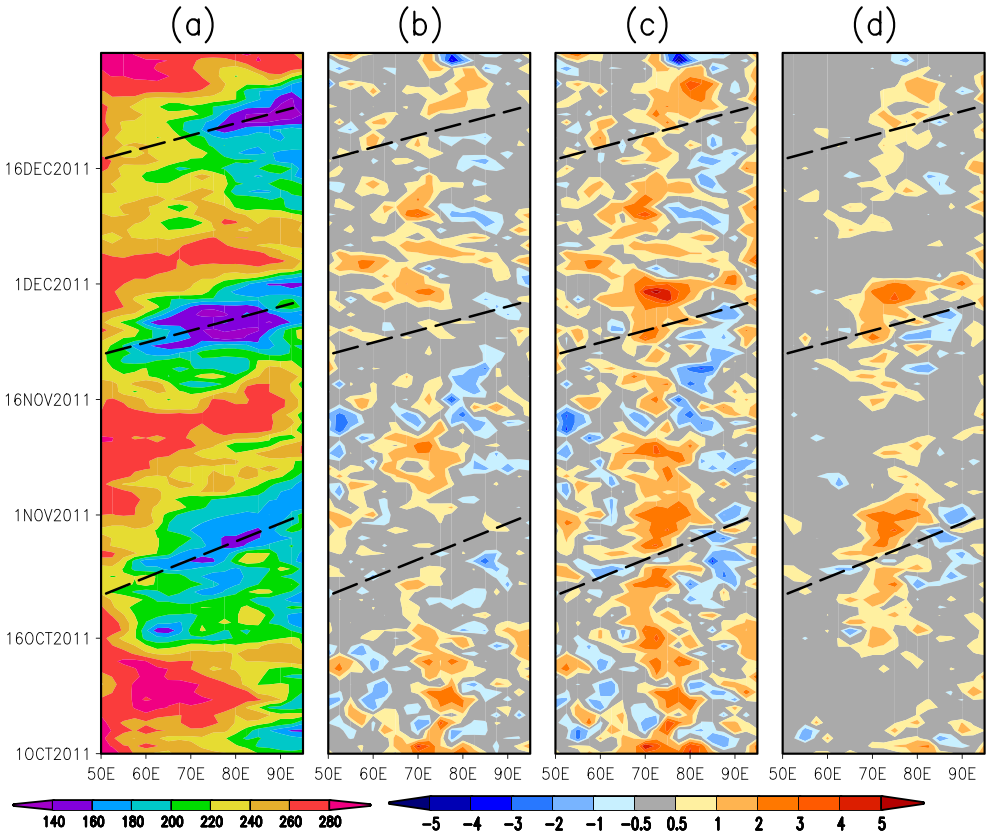

Figure 8. The Hovmöller diagram of (a) all-sky OLR averaged between 5°S and 10°N from the control Fu-Liou experiment. (b) Same as Figure 8a but for the all-sky OLR differences between the DYNAMO and Control Fu-Liou experiments (DYNAMO minus Control). (c) Same as Figure 8b but for clear-sky OLR. (d) Same as Figure 8b but for TOA longwave CRE. The black dashed lines indicate OLR minima axes. Units are in W m^{-2}.

Given that the *Q* and *T* improvement from the DYNAMO observation assimilation mainly occurs in their vertical profiles (e.g., Figure 3), it is of interest to further investigate the separate roles of *Q* and *T* improvement, as well as their improvement at different vertical pressure ranges, in contributing to the overall changes in the computed daily longwave flux. In particular, we are interested in assessing the separate contribution from the warming and moistening in the upper troposphere, the cooling and drying in the middle and mid-upper troposphere, and the warming and moistening in the lower troposphere—a reflection of improved representation of low-level moist processes in the reanalysis compared to that in the GEOS 5 AGCM. Such assessment can provide a better understanding of how an improved representation of observed processes in the GMAO reanalysis may subsequently improve the CERES SYN1deg-like daily longwave estimates.

The assessment was carried out by contrasting the results from the control Fu-Liou experiment with those of the Fu-Liou experiments in which we only vary *T* or *Q* in certain vertical pressure ranges (Q, Qlo, Qmi, Qhi, T, Tlo, Tmi, and Thi in Table 1). Given the dependence of all-sky OLR on dry and wet periods, we performed the assessment for dry and wet periods separately. Here wet periods refer to periods during which deep convection occurred, specifically, 20 October to 4 November, 22–30 November, and 16–27 December 2011, whereas dry periods refer to the remaining days during 1 October to 31 December 2011. Figure 10 summarizes the results for all-sky condition averaged over the central tropical Indian Ocean (70°E–82°E, 5°S–10°N). Note that the values averaged over the central tropical Indian Ocean are smaller than those over the DYNAMO stations, as the impact of the DYNAMO observations is the greatest over the DYNAMO stations and reduces elsewhere. Figure 10a shows that the changes in *Q* and *T* only affect the computed all-sky OLR during dry periods, and the effect of the *Q* changes dominates. The overall effect of *Q* changes on all-sky OLR during dry periods (0.4 W m^{-2}) is a result of an OLR increase from drying the middle troposphere (1.7 W m^{-2}) dominating over OLR decreases from moistening the lower troposphere (−0.6 W m^{-2}) and upper troposphere (−0.7 W m^{-2}).

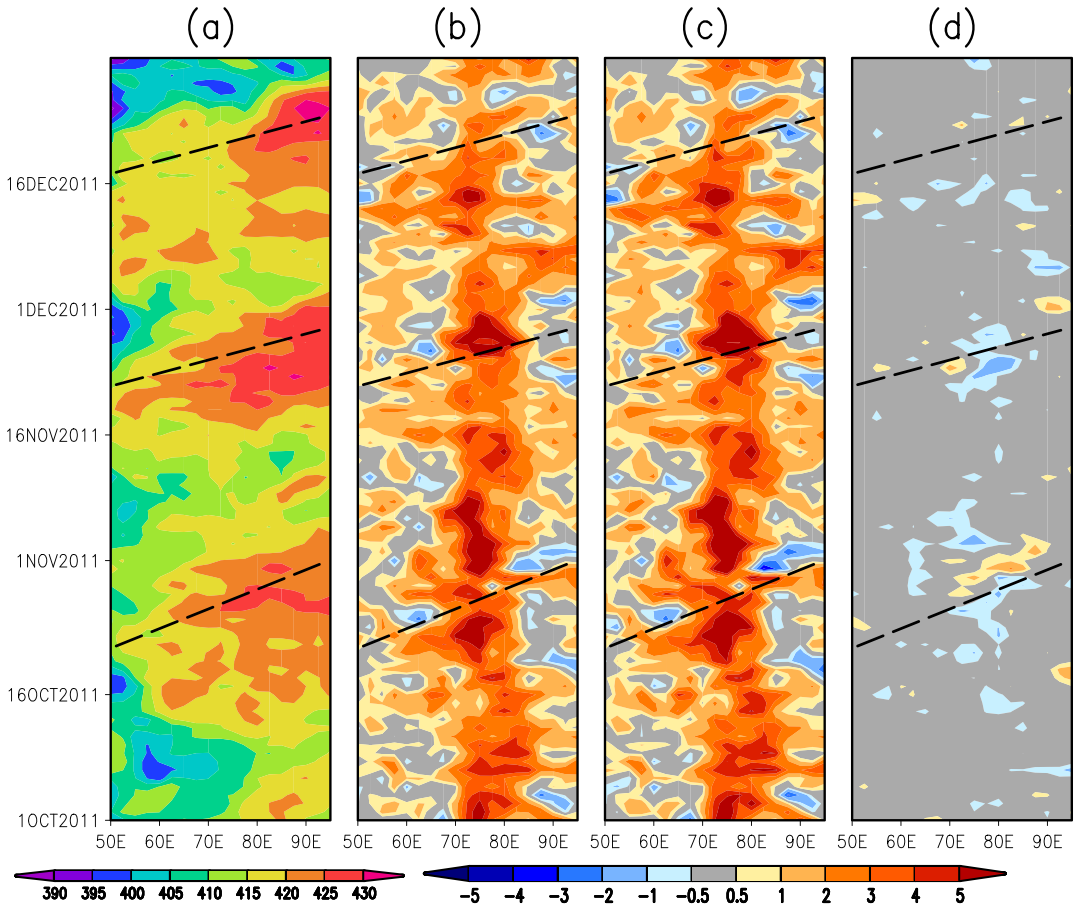

Figure 9. The Hovmöller diagram of (a) surface downward all-sky longwave averaged between 5°S and 10°N from the control Fu-Liou experiment. (b) Same as Figure 9a but for surface downward all-sky longwave differences between the DYNAMO and control Fu-Liou experiments (DYNAMO minus control). (c) Same as Figure 9b but for surface downward clear-sky longwave. (d) Same as Figure 9b but for surface longwave CRE. The black dashed lines indicate OLR minima axes. Units are in W m^{-2}.

Consistent with Figure 9, the effects of *Q* and *T* changes on all-sky surface downward longwave during wet periods do not differ much from those during dry periods (Figure 10c). The increases in the computed surface downward longwave are contributed by changes in both *Q* and *T*, which account for about one third and two thirds of the total increase, respectively. The area-mean increase of the computed surface downward longwave due to the *Q* changes over the central tropical Indian Ocean (70°E–82°E, 5°S–10°N) mainly results from an increase (1.7 W m^{-2}) from the moistened lower troposphere dominating over a decrease from the drying of the middle troposphere (−0.8 W m^{-2}). The increase in the estimate of surface downward longwave flux due to *T* changes is dominated by the warming in the lower troposphere.

Associated with the above changes in the computed longwave at the TOA (Figure 10a) and surface (Figure 10c), the computed atmospheric longwave radiative cooling averaged over the central tropical Indian Ocean (70°E–82°E, 5°S–10°N) increases by 2.5 W m^{-2} during dry periods and 3.0 W m^{-2} during wet periods, which are primarily contributed by the lower tropospheric warming. While the net effect of the *Q* changes is small (a mean increase of 0.4 W m^{-2} during dry periods and 0.9 W m^{-2} during wet periods), it is a result of strong compensation between the longwave decrease from drying the middle troposphere and the longwave increase from moistening the lower troposphere and the upper troposphere.

3.3. Relevance to CERES SYN1deg and EBAF-Surface Data Production

Do the above differences in the computed surface and atmospheric longwave fluxes between the DYNAMO and control Fu-Liou experiments represent an improvement? While there are no daily global observations

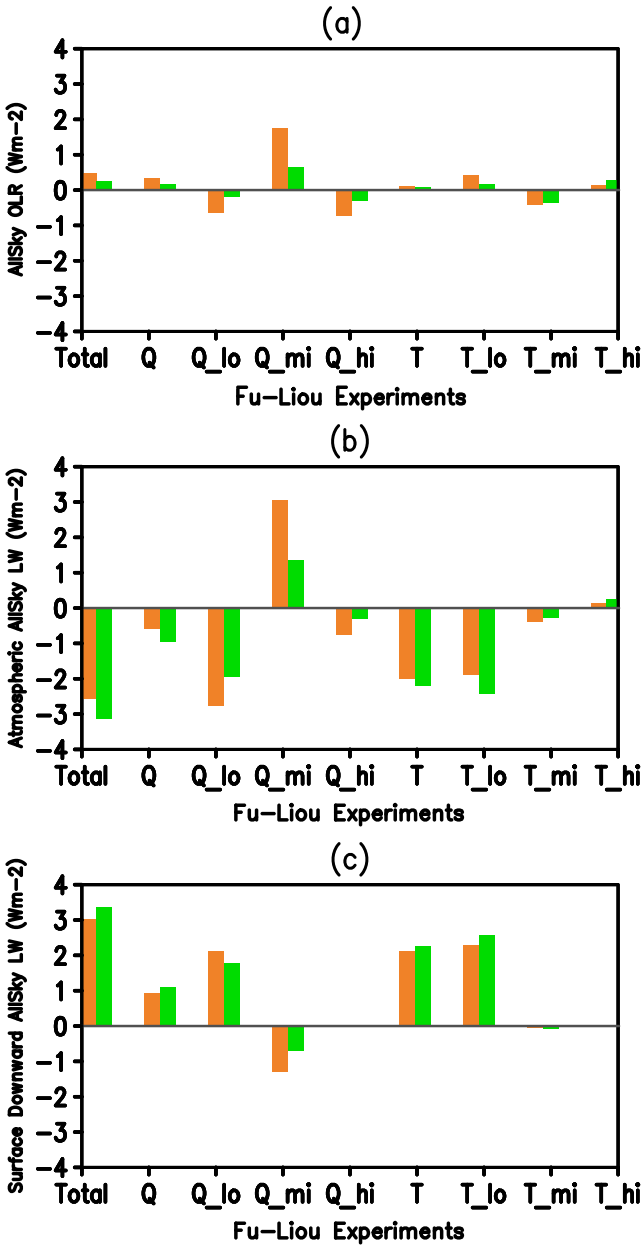

Figure 10. (a) The mean difference of all-sky OLR averaged over the central tropical Indian Ocean (70°E–82°E, 5°S–10°N) between the control Fu-Liou experiment and the sensitivity Fu-Liou experiments in Table 1, averaged over dry periods (brown bar) and wet periods (green bar) during 1 October to 31 December 2011. (b) Same as Figure 10a but for atmospheric all-sky longwave flux. (c) Same as Figure 10a but for surface downward all-sky longwave flux. Units are in W m^{-2}.

available for a direct validation, we can make an inference by examining whether these differences improve the CERES SYN1deg and EBAF-Surface longwave estimates over the DYNAMO stations.

We first evaluate the control reanalysis, the DYNAMO reanalysis, and the AIRS data by comparing their vertical profiles of atmospheric humidity and temperature against those in the quality-controlled DYNAMO gridded observations. Here the AIRS data are included in the evaluation, mainly because in the CERES EBAF-Surface data production, the AIRS atmospheric humidity and temperature profiles are used to determine the uncertainty of those in the GMAO reanalysis used as well as to perform an initial correction of upper tropospheric humidity. Figure 11 shows the comparison over the 1°×1° gridbox that contains Gan Island (73°E, 0.7°S), one of the key DYNAMO stations, for October 2011. Relative to the DYNAMO observations, the control reanalysis shows a wet bias in the middle troposphere, with a peak of 0.6 g kg^{-1} at 450 hPa, and dry biases in the lower troposphere (−1.0 g kg^{-1}) and near the surface (−1.1 g kg^{-1}). The control reanalysis also displays a warm bias that peaks at 250 hPa (0.8 K) as well as discrete cold biases in the lower troposphere (−1 K at 700 hPa and −1.8 K at 925 hPa). The assimilation of the DYNAMO observations reduces the above humidity bias in the control reanalysis by about 40% throughout much of the troposphere and the temperature bias by 40%–70% below 500 hPa, consistent with Figure 3. By comparison, the AIRS data show dry and warm biases in the middle troposphere, with a peak of −0.4 g kg^{-1} and 0.6 K at about 500 hPa. These biases could be due to the limited AIRS data sampling during the second half of October 2011 when a MJO event occurred. Near surface, the AIRS data display a dry bias of −1 g kg^{-1} and a cold bias of −1.1 K. While not apparent in Figure 11a, the AIRS humidity bias in the upper troposphere is considerably smaller than those in the control and DYNAMO reanalyses.

As a result of the above improved humidity and temperature profiles from the DYNAMO data assimilation (Figure 11), the DYNAMO Fu-Liou experiment shows a considerable improvement over the control

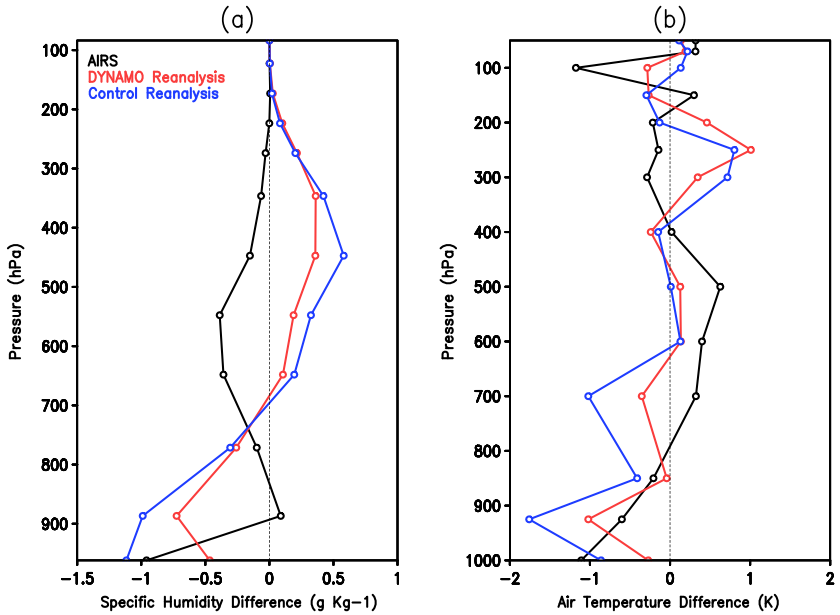

Figure 11. The differences in the vertical profiles of (a) specific humidity (g kg^{-1}) and (b) air temperature (K) between the DYNAMO in situ observations and the AIRS (black line), the DYNAMO reanalysis (red line), and the control reanalysis (blue line), for the 1°×1° gridbox that contains Gan Island (73°E, 0.7°S) for October 2011.

experiment in SYN1deg-like longwave estimates at both the TOA and surface (Figure 12). For both clear-sky and all-sky conditions, the assimilation of the DYNAMO observations reduces the underestimation of OLR from 6.9 W m^{-2} in the control experiment to 4.8 W m^{-2} in the DYNAMO experiment (Figure 12b). The impact of the DYNAMO observation assimilation is more notable at the surface, where the underestimation of surface downward longwave is reduced from 5.8 W m^{-2} in the control experiment to 1.1 W m^{-2} in the DYNAMO experiment (Figure 12d). The subsequent contribution to improving the CERES EBAF-Surface longwave estimates can be inferred by comparing the AIRS-based longwave estimates with those using the DYNAMO reanalysis (Figure 12). Benefiting from the good quality of its atmospheric humidity, particularly above 500 hPa (Figure 11a), the AIRS agrees with the DYNAMO observations in the computed OLR, with an overestimation of only 1.4 W m^{-2}. This supports the use of the AIRS humidity and temperature for the upper humidity correction as well as the TOA irradiance constrainment in the CERES EBAF-Surface Ed2.8 data production. The AIRS, however, shows a notable underestimation of 6.0 W m^{-2} in surface downward longwave, which is even larger than the bias in the control experiment. The notable AIRS-based underestimation is due mainly to its cold bias (−1.1 K) near surface (Figure 11b), where the temperature biases can be most efficient in affecting the surface downward longwave, relative to the temperature biases at atmospheric layers further above [*Rose et al.*, 2015]. Since the adjustment of surface, atmospheric, and cloud properties performed in the CERES EBAF-Surface Ed2.8 data production targets matching the corresponding computed SYN1deg fluxes with the CERES-derived fluxes only at the TOA, the improvements in the SYN1deg-like surface downward longwave estimates (from the DYNAMO observation assimilation) are expected to propagate to the EBAF-Surface data. Note that while not shown here, the results for other DYNAMO stations and months are overall similar to those in Figures 11 and 12. In addition, the TOA and surface CREs are comparable among the four Fu-Liou experiments (Figure 12), as they use identical cloud properties from the SYN1deg Ed3A.

As a reference, we also examined observed surface downward longwave radiant flux using data from Radiative Flux Analysis as part of the Atmospheric Radiation Measurement MJO Investigation Experiment on Gan Island [*Long*, 2016]. The observed monthly mean surface downward all-sky (clear-sky) longwave at the Gan Island site for October 2011 is 421.1 W m^{-2} (403.7 W m^{-2}), which is considerably greater (smaller) than the estimates based on Fu-Liou radiative transfer calculations for the 1°×1° gridbox that contains Gan Island (Figure 12c). The observed surface longwave CRE (17.4 W m^{-2}) at the Gan Island site is also notably greater than the 1°×1° gridbox-based estimates (Figure 12d). These discrepancies are not surprising, as

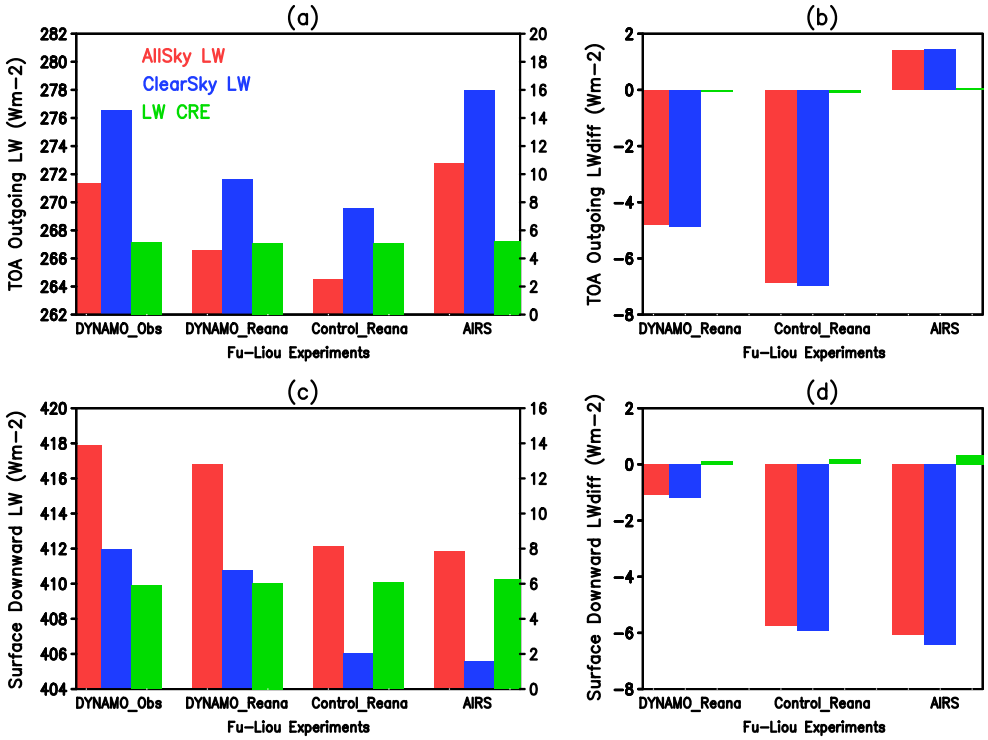

Figure 12. (a) The all-sky OLR (red bar), clear-sky OLR (blue bar), and TOA LW CRE (green bar) estimated based on Fu-Liou radiative transfer computations that use monthly mean cloud and surface properties from the Ed3A SYN1deg and atmospheric state variables from (left) the DYNAMO gridded observations, (second from left) the DYNAMO reanalysis, (third from left) the control reanalysis, and (fourth from left) the AIRS, for the 1° × 1° gridbox that contains Gan Island (73°E, 0.7°S) for October 2011. (b) Same as Figure 12a but for the differences from the Fu-Liou results for the DYNAMO gridded observations. (c) Same as Figure 12a but for surface downward longwave. (d) Same as Figure 12b but for surface downward longwave. Units are in W m^{-2}.

surface and atmospheric properties over islands usually do not adequately represent those of the rest regions within a 1° × 1° gridbox [*Kato et al.*, 2012].

4. Summary and Conclusion

This study investigates the impact of assimilating quality-controlled DYNAMO in situ observations in the GMAO reanalysis system and the corresponding influence on the CERES SYN1deg-like daily surface, in-atmosphere, and TOA radiative flux estimates. The impact of including the DYNAMO observations in a recent version of GMAO DAS is examined by comparing two 1° GMAO reanalyses that assimilate global observations with and without the DYNAMO in situ observations, referred to as the DYNAMO reanalysis and the control reanalysis, respectively. The comparison of the two reanalyses shows that the assimilation of the DYNAMO in situ observations over the central tropical Indian Ocean (1 October 2011 to 31 March 2012) considerably improves local air temperature and specific humidity, particularly their vertical profiles, in the GMAO reanalysis. Notably, the assimilation of the DYNAMO observations significantly moistens and warms the lower troposphere and upper troposphere, and dries and cools the mid-upper troposphere, bringing the reanalysis closer to the DYNAMO observations. To assess the influence of assimilating the DYNAMO measurements on surface, in-atmosphere, and TOA radiative flux estimates, a series of Fu-Liou radiative transfer calculations for the DYNAMO period (1 October to 31 December 2011) were performed, in which daily Q and T are taken from either the DYNAMO reanalysis or the control reanalysis, with the rest of the daily input fields (e.g., cloud properties) taken from the CERES SYN1deg Ed3A. The results show that the effect on daily surface and atmospheric radiation estimates mainly occurs in the longwave flux over and near the DYNAMO stations; the impact on SW is negligible. Over the DYNAMO region, the computed daily surface downward longwave flux estimates increase by about 5 W m^{-2} for both clear-sky and all-sky conditions,

which are primarily due to the warming and moistening in the lower troposphere. At the TOA, the computed daily clear-sky OLR increases by 2–3 W m^{-2} throughout much of the period, whereas the computed all-sky OLR shows such increases (by 2–3 W m^{-2}) during dry periods only, due to the fact that all-sky OLR is largely determined by deep convective clouds rather than changes in *T* and *Q* during wet periods. These changes in OLR estimates result from the drying in the middle troposphere partially offset by the moistening in the upper troposphere and lower troposphere. In the atmosphere, the estimated atmospheric longwave radiative cooling over the tropical Indian Ocean enhances by about 5 W m^{-2} during deep convective periods and 7–8 W m^{-2} during dry suppressed periods. The above longwave estimates over select DYNAMO stations were evaluated by comparing them against those from a Fu-Liou experiment in which the *T* and *Q* from the DYNAMO gridded observations were used. The evaluation confirms that the DYNAMO observation assimilation in the GMAO reanalysis considerably improves the SYN1deg-like longwave estimates at both the TOA and surface over the DYNAMO region.

It is worth noting that while this study is based on reanalyses produced with a recent GMAO AGCM and DAS (tag: GEOSadas-5_12_4), the findings are in general applicable to the CERES SYN1deg Ed3A, which uses a GMAO reanalysis produced with an older version of the GEOS 5 DAS and AGCM (tag: GEOSadas-4_1 prior to January 2008 and GEOSadas-5_2_0 on and after January 2008). The lower tropospheric cold and dry biases are also apparent in these older versions of the GMAO reanalysis (not shown), which can contribute to an underestimation of surface downward longwave radiation in the SYN1deg Ed3A. In fact, an evaluation of surface downward longwave flux using surface observations at 48 ocean buoy sites within 30°S-30°N shows a monthly mean bias of −3.6 W m^{-2} for the SYN1deg Ed3A and −3.5 W m^{-2} for the EBAF-Surface Ed2.7 [*Rutan et al.*, 2015]. This study suggests that these underestimations of the observed surface downward longwave flux over the tropical ocean in the SYN1deg Ed3A and Surface-EBAF Ed2.7 can be considerably reduced by using an improved GMAO reanalysis that has little or reduced low-level cold and dry biases. Currently, plans are in place at GMAO to improve the GEOS 5 AGCM by introducing a new shallow convection scheme in order to explicitly treat shallow convection processes and correct the lower tropospheric cold and dry biases (Andrea Molod, personal communication, 2016). This, along with advances in GMAO data assimilation system and inclusion of observations from many state-of-the-art data sources, will lead to improved GMAO reanalysis and contribute to improving future versions of CERES SYN1deg and EBAF-Surface data.

Acknowledgments

This work has been supported by the NOAA Earth System Science (ESS) program (NA13OAR4310162) and the NASA Clouds and the Earth's Radiant Energy System (CERES) project. We would like to thank David Doelling, Seiji Kato, and Fred Rose for their helpful discussions on the CERES SYN1deg Ed3A and EBAF-Surface Ed2.8 data production and Jennifer Wei for information on the AIRS data hosted at the NASA Goddard Earth Sciences Data and Information Services Center (GES DISC). We also would like to thank two anonymous reviewers for their comments and suggestions, which have greatly improved the paper. The CERES data sets were obtained from http://ceres.larc.nasa.gov/compare_-products.php. The CSU-DYNAMO gridded analyses were downloaded from http://johnson.atmos.colostate.edu/dynamo/products/gridded/index.html, and the AIRS data were obtained from the NASA GES DISC. The observed surface downward longwave at the Gan Island site was obtained from the Amie-Gan data set at http://www.archive.arm.gov/discovery/#v/results/s/fiop::amf2011amie-gan.

References

Achuthavarier, D., H. Wang, S. D. Schubert, and M. Sienkiewicz (2017), Impact of DYNAMO observations on NASA GEOS-5 reanalyses and the representation of MJO initiation, *J. Geophys. Res. Atmos.*, *122*, 179–201, doi:10.1002/2016JD025363.

Aumann, H. H., et al. (2003), AIRS/AMSU/HSB on the aqua mission: Design, science objectives, data products, and processing systems, *IEEE Trans. Geosci. Remote Sens.*, *41*(2), 253–264, doi:10.1109/tgrs.2002.808356.

Bacmeister, J. T., M. J. Suarez, and F. R. Robertson (2006), Rain reevaporation, boundary layer–convection interactions, and pacific rainfall patterns in an AGCM, *J. Atmos. Sci.*, *63*, 3383–3403.

Bloom, S., L. Takacs, A. DaSilva, and D. Ledvina (1996), Data assimilation using incremental analysis updates, *Mon. Weather Rev.*, *124*, 1256–1271.

Bosilovich, M. G., et al. (2015), MERRA-2: Initial evaluation of the climate, NASA/TM–2015–104606, vol. 43, 139 pp.

Chahine, M. T., et al. (2006), AIRS: Improving weather forecasting and providing new data on greenhouse gases, *Bull. Am. Meteorol. Soc.*, *87*(7), 911–926, doi:10.1175/bams-87-7-911.

Ciesielski, P. E., et al. (2014a), Quality-controlled upper-air sounding dataset for DYNAMO/CINDY/AMIE: Development and corrections, *J. Atmos. Oceanic Technol.*, *31*, 741–764.

Ciesielski, P. E., R. H. Johnson, K. Yoneyama, and R. K. Taft (2014b), Mitigation of Sri Lanka island effects in Colombo sounding data and its impact on DYNAMO analyses, *J. Meteorol. Soc. Jpn.*, *92*, 385–405.

Del Genio, A. D., and Y. Chen (2015), Cloud-radiative driving of the Madden-Julian oscillation as seen by the A-Train, *J. Geophys. Res. Atmos.*, *120*, 5344–5356, doi:10.1002/2015JD023278.

Doelling, D. R., N. G. Loeb, D. F. Keyes, M. L. Nordeen, D. Morstad, C. Nguyen, B. A. Wielicki, D. F. Young, and M. Sun (2013), Geostationary enhanced temporal interpolation for CERES flux products, *J. Atmos. Oceanic Technol.*, *30*, 1072–1090.

Fu, Q., and K. N. Liou (1992), On the correlated k-distribution method for radiative transfer in nonhomogeneous atmospheres, *J. Atmos. Sci.*, *49*, 2139–2156.

Hagos, S., Z. Feng, K. Landu, and C. N. Long (2014), Advection, moistening, and shallow-to-deep convection transitions during the initiation and propagation of Madden-Julian Oscillation, *J. Adv. Model. Earth Syst.*, *6*, 938–949, doi:10.1002/2014MS000335.

Johnson, R. H., and P. E. Ciesielski (2013), Structure and properties of Madden–Julian Oscillations deduced from DYNAMO sounding arrays, *J. Atmos. Sci.*, *70*, 3157–3179.

Kato, S., N. G. Loeb, D. A. Rutan, F. G. Rose, S. Sun-Mack, W. F. Miller, and Y. Chen (2012), Uncertainty estimate of surface irradiances computed with MODIS-, CALIPSO-, and CloudSat-derived cloud and aerosol properties, *Surv. Geophys.*, doi:10.1007/s10712-012-9179-x.

Kato, S., N. G. Loeb, F. G. Rose, D. R. Doelling, D. A. Rutan, T. E. Caldwell, L. Yu, and R. A. Weller (2013), Surface irradiances consistent with CERES-derived top-of-atmosphere shortwave and longwave irradiances, *J. Clim.*, *26*, 2719–2740, doi:10.1175/JCLI-D-12-00436.1.

Kim, D., et al. (2014), Process-oriented MJO simulation diagnostic: Moisture sensitivity of simulated convection, *J. Clim.*, *27*, doi:10.1175/JCLI-D-13-00497.1.

Koster, R. D., M. J. Suarez, and M. Heiser (2000), Variance and predictability of precipitation at seasonal-to-interannual timescales, *J. Hydrometeorol.*, *1*, 26–46.
Lin, S.-J. (2004), A vertically Lagrangian finite-volume dynamical core for global models, *Mon. Weather Rev.*, *132*, 2293–2307.
Loeb, N. G., B. A. Wielicki, D. R. Doelling, G. L. Smith, D. F. Keyes, S. Kato, N. Manalo- Smith, and T. Wong (2009), Toward optimal closure of the Earth's top-of-atmosphere radiation budget, *J. Clim.*, *22*, 748–766, doi:10.1175/2008JCLI2637.1.
Loeb, N. G., J. M. Lyman, G. C. Johnson, R. P. Allan, D. R. Doelling, T. Wong, B. J. Soden, and G. L. Stephens (2012), Observed changes in top-of-the-atmosphere radiation and upper-ocean heating consistent within uncertainty, *Nat. Geosci.*, *5*, 110–113, doi:10.1038/NGEO1375.
Long C. N. (2016), Atmospheric Radiation Measurement Madden-Julian Oscillation investigation experiment field campaign report, *U.S. Dep. of Energy Rep. (DOE/SC-ARM-16-039)*. [Available at https://www.arm.gov/publications/programdocs/doe-sc-arm-16-039.pdf.]
Mapes, B. E., and J. T. Bacmeister (2012), Diagnosis of tropical biases and the MJO from patterns in the MERRA analysis tendency fields, *J. Clim.*, *25*, 6202–6214.
Molod, A., L. Takacs, M. Suarez, J. Bacmeister, I.-S. Song, and A. Eichmann (2012), The GEOS-5 atmospheric general circulation model: Mean climate and development from MERRA to Fortuna, *Tech. Rep. Ser. on Global Modeling and Data Assimilation*, vol. 28.
Moorthi, S., and M. J. Suarez (1992), Relaxed Arakawa Schubert: A parameterization of moist convection for general circulation models, *Mon. Weather Rev.*, *120*, 978–1002.
Nagarajan, B., and A. Aiyyer (2004), Performance of the ECMWF operational analyses over the tropical Indian Ocean, *Mon. Weather Rev.*, doi:10.1175/1520-0493(2004)132<2275:POTEOA>2.0.CO;2.
Nuss, W. A., and D. W. Titley (1994), Use of muliquadric interpolation for meteorological objective analysis, *Mon. Weather Rev.*, *122*, 1611–1631.
Rienecker, M. M., et al. (2008), The GEOS-5 data assimilation system—Documentation of versions 5.0.1, 5.1.0, and 5.2.0, *Tech. Rep. Ser. on Global Modeling and Data Assimilation*, vol. 27.
Rose, F. G., D. A. Rutan, T. P. Charlock, G. L. Smith, and S. Kato (2013), An algorithm for the constraining of radiative transfer calculations to CERES-observed broadband top-of-atmosphere irradiance, *J. Atmos. Oceanic Technol.*, *30*, 1091–1106.
Rose, F. G., S. Kato, and T. Caldwell (2015), MERRA-2/AIRS/MODIS temperature/humidity comparisons, *The 23rd CERES-II Science Team Meeting*, Hampton, Va. [Available at https://ceres.larc.nasa.gov/documents/STM/2015/05/38_Rose_Kato.GMAO_AIRS.Final.CERES_STM.May5_2015.pdf.]
Rutan, D. A., S. Kato, D. R. Doelling, F. G. Rose, L. T. Nguyen, T. E. Caldwell, and N. G. Loeb (2015), CERES synoptic product: Methodology and validation of surface radiant flux, *J. Atmos. Oceanic Technol.*, *32*(6), 1121–1143.
Sobel, A. H., and E. D. Maloney (2012), An idealized semi-empirical framework for modeling the Madden-Julian Oscillation, *J. Atmos. Sci.*, *69*, 1691–1705.
Sobel, A. H., and E. D. Maloney (2013), Moisture modes and the eastward propagation of the MJO, *J. Atmos. Sci.*, *70*, 187–192.
Sobel, A., S. Wang, and D. Kim (2014), Moist static energy budget of the MJO during DYNAMO, *J. Atmos. Sci.*, *71*, 4276–4291.
Tian, B., E. Manning, E. J. Fetzer, E. Olsen, S. Wong, J. Susskind, and L. Iredell (2013a), AIRS/AMSU/HSB version 6 Level 3 product user guide. [Available online at http://disc.sci.gsfc.nasa.gov/AIRS/documentation/v6_docs/v6releasedocs-1/V6_L3_User_Guide.pdf.]
Tian, B., E. Fetzer, B. Kahn, J. Teixeira, E. Manning, and T. Hearty (2013b), Evaluating CMIP5 models using AIRS tropospheric air temperature and specific humidity climatology, *J. Geophys. Res. Atmos.*, *118*, 114–134, doi:10.1029/2012JD018607.
Tokioka, T., K. Yamazaki, A. Kitoh, and T. Ose (1988), The equatorial 30–60 day oscillation and the Arakawa-Schubert penetrative cumulus parameterization, *J. Meteorol. Soc. Jpn.*, *66*, 883–901.
Waliser, D. E. (2011), Predictability and forecasting, in *Intraseasonal Variability of the Atmosphere-Ocean Climate System*, edited by W. K. M. Lau and D. E. Waliser, pp. 433–476, Springer, Heidelberg, Germany.
Wang, S., A. H. Sobel, and Z. Kuang (2013), Cloud-resolving simulation of TOGA-COARE using parameterized large-scale dynamics, *J. Geophys. Res. Atmos.*, *118*, 6290–6301, doi:10.1002/jgrd.50510.
Wang, S., A. H. Sobel, and J. Nie (2016), Modeling the MJO in a cloud-resolving model with parameterized large-scale dynamics: Vertical structure, radiation, and horizontal advection of dry air, *J. Adv. Model. Earth Syst.*, *8*, 121–139, doi:10.1002/2015MS000529.
Yoneyama, K., C. Zhang, and C. N. Long (2013), Tracking pulses of the Madden–Julian Oscillation, *Bull. Am. Meteorol. Soc.*, *94*, 1871–1891.
Zhang, C. (2005), Madden-Julian Oscillation, *Rev. Geophys.*, *43*, RG2003, doi:10.1029/2004RG000158.